Exploiting Energy Harvesting for Low-Power Wide-Area System with and without Cooperative communications

Xuan Nam Tran, Van-Phuc Hoang, Ba Cao Nguyeng,

Abstract

This paper studies the ergodic capacity (EC) of full-duplex (FD) amplify-and-forward (AF) and decode-and-forward (DF) relay system with energy harvesting (EH) for vehicle-to-vehicle (V2V) communications. Unlike previous works on FD-EH systems, we consider the case that both relay and destination are mobile vehicles while the source is a static base station. We mathematically derive the exact closed-form expressions of ECs of both AF and DF protocols of the considered FD-EH-V2V relay system over cascade (double) Rayleigh fading. Our numerical results show that the ECs in the case of V2V communication system are reduced compared to those in the case of stationary nodes. Also, with a specific value of residual self-interference (RSI), the ECs of the considered FD-EH-V2V relay system can be higher or lower than those of half-duplex (HD)-EH-V2V system, depending on the average transmission power of the source. Furthermore, when the transmission power of source and RSI are fixed, the ECs of the considered system can achieve peak values by using optimal EH time duration. On the other hand, the ECs of both AF and DF protocols reach the capacity floors in the high signal-to-noise ratio (SNR) regime due to the RSI impact. Also, the effect of RSI dominates the impact of cascade Rayleigh fading in the high SNR regime. Finally, we validate our analysis approach through Monte-Carlo simulations.

Index Terms

Vehicle-to-vehicle communications, cascade Rayleigh fading channels, full-duplex, energy harvesting, ergodic capacity.

I. Introduction

In the age of Industry 4.0, various new techniques have been fast developed to satisfy the requirements of capacity and energy consumption of the future wireless networks such as the fifth-generation (5G) and beyond (B5G) [1]–[3]. In addition, the emergence of trillions of Internet-of-Things (IoT) devices in the world requires devices to consume less energy and transmit data at a higher rate [3], [4]. Therefore, energy harvesting (EH) from radio frequency (RF) signal has been used to deal with these

Corresponding author, Xuan Nam Tran, is with Le Quy Don Technical University, Ha Noi, Vietnam (e-mail: namtx@mta.edu.vn).

Van-Phuc Hoang is with Le Quy Don Technical University, Ha Noi, Vietnam (e-mail: phuchv@mta.edu.vn).

Ba Cao Nguyen is with Telecommunications University, Khanh Hoa, Vietnam (e-mail: nguyenbacao@tcu.edu.vn).

issues [4], [5]. Together with the traditional energy grid, EH can help to fulfill the energy requirements for different elements of 5G networks, including sensors in the IoT, mobile devices, heterogeneous networks (HetNets), relays in device-to-device (D2D) systems, and computing servers [3]. Additionally, the emergence of advanced materials and hardware designs helps realize the EH circuits for small portable consumer electronic devices in the IoT. Furthermore, RF signals can be transmitted over the air all the time. Thus, EH from RF signals can provide stable energy for wireless devices that consume low power such as IoTs, sensor, and the remote area communication used in 5G and B5G systems [1], [3].

Meanwhile, full-duplex (FD) is a promising technique for achieving high spectral efficiency in wireless systems thanks to its capability to allocate the transmitted and received radio signals of a communication node on the same frequency and in the same time slot. Ideally, FD transmission increases the spectral efficiency twice compared to traditional half-duplex (HD) transmission. As a promising technology for next-generation (5G and B5G) wireless networks, FD wireless not only has the potential to double the spectrum efficiency in the physical layer, but can also enhance the performance of wireless systems such as reducing feedback delay, end-to-end delay, and congestion, improving the network secrecy and efficiency, and increasing the throughput and spectrum usage flexibility [6], [7]. Overall, it is envisaged that FD communications technology can be adopted in the near future in a number of scenarios and applications, such as throughput enhancement in the sub-6-GHz band, supporting ultra-low delay communication, small and dense cells [6], [8]–[10].

In the literature, various works have combined of EH and FD techniques in a wireless communication system to solve the battery and spectrum efficiency issues [8], [10], [11]. The mathematical analysis and the experimental measurements have been applied for investigating the performance of FD-EH systems. Specifically, the mathematical analysis is used to derive expressions of outage probability (OP), symbol error rate (SER), bit error rate (BER), and ergodic capacity (EC) of the FD-EH systems [8], [10]–[13]. Based on these obtained mathematical expressions, the system behavior is analyzed under the effects of different parameters such as the residual self-interference (RSI) induced by FD transmission mode, the time switching ratio, and the channel conditions. It is found that optimal power allocation for FD transmission mode and optimal time switching ratio for EH can improve the system performance significantly [14]–[16]. Furthermore, the EC of the FD-EH system is generally higher than that of the HD-EH system for specific RSI values. Experimental measurements have also been widely used to evaluate the algorithms and solutions used to improve the performance of FD-EH systems [12], [17]–[19]. By applying the optimization problem in a non-convex form, the FD-EH system's system power is minimized and better than that of the HD-EH system [19], and the sum rate and energy efficiency are maximized [18]. As a result, most of the works about FD-EH systems have analyzed RSI and other system parameters' impacts and then proposed solutions to reduce OP, SER, and enhance EC and energy efficiency. Furthermore, exploiting FD-EH systems in different scenarios such as cognitive radio (CR), spatial

modulation (SM), cooperative communication has been widely carried out.

Recently, both FD and EH techniques are deployed in vehicle-to-vehicle (V2V) communication systems because of their various advantages in V2V environments. Thanks to FD and EH techniques, the V2V communication systems can reduce the delay time for signal transmission between vehicles and the power supply limitation problem [20], [21]. Hence, FD-EH-V2V relay system can be applied for the intelligent transportation systems (ITS) and the road safety applications [8], [10], [20]. Specifically, the onboard unit was proposed in [20] to supply the energy for FD-V2V communications from the vehicle engine. Although this scheme could solve the energy issues, applying EH for V2V communication systems still becomes an inevitable trend thanks to many advantages of EH technique. In recent reports, the OP, SER, and throughput of the FD-EH-V2V relay systems were obtained to investigate the system performance and evaluate the effects of several system parameters such as RSI, time switching ratio, and channel characteristics [8], [10]. In particular, papers [8] and [10] derived the OP and SER expressions of FD-EH-V2V relay systems with AF and DF relaying protocols, respectively. However, the EC expressions of these FD-EH-V2V relay systems were not obtained. Meanwhile, we always want to get the lowest OP/SER and the highest EC for wireless communication systems. Therefore, investigating OP/SER and ignoring EC when analyzing the performance of wireless communication systems may result in inaccurate conclusions on the system behaviors. Specifically, experiments and measurements indicate that the cascade (double) Rayleigh fading distribution best describes the channels between vehicle nodes [21], [22], while the traditional channels such as Nakagami, Rician, and Rayleigh cannot fully model the V2V communication channel. It is shown that, under the effects of RSI and cascade Rayleigh fading channel, the OP and SER of the FD-EH-V2V relay systems reach the error floor faster in the high SNR regime. Additionally, cascade Rayleigh fading channel makes the derivation of closed-form expressions more difficult than Nakagami, Rician, and Rayleigh channels [8], [10], [22], leading to a lack of mathematical analysis of FD-EH-V2V relay systems over cascade Rayleigh fading channels.

As the above discussions, the main benefit of FD transmission is high capacity compared with HD one. However, mathematical analysis of the EC of FD-EH-V2V relay systems under the effect of cascade Rayleigh fading has not been investigated yet. Meanwhile, EH and FD techniques in V2V communication systems are inevitable because these techniques can solve various issues in traditional V2V systems. Mainly, EH is an effective method for power supply in the case that the wireline power supply may not be deployed for moving vehicles. At the same time, the FD can improve the performance of safety applications for V2V systems. Therefore, it is required to mathematically analyze the ECs of the FD-EH-V2V relay system for both AF and DF protocols to evaluate the system behavior. This observation motivates us to perform a mathematical analysis of the ECs of the FD-EH-V2V relay system with AF/DF protocols over cascade Rayleigh fading channels. In our paper, we focused on analyzing the impacts of the cascade Rayleigh fading channel, RSI, and time switching ratio on the ECs of FD-EH-V2V

relay system with AF/DF protocol by deriving the exact closed-form expressions of these attributes and comparing with those in the case of Rayleigh fading channel, perfect SIC, and HD system. So far, this is the first work deriving the EC expressions of FD-EH-V2V relay system over cascade Rayleigh fading channels. It is noted that, exploiting EH from RF signals provides stable energy supply for low-power consumption networks such as IoTs, wireless sensor networks, extremely remote area communications used in 5G and B5G systems [4], [19], and vehicular networks [23]. Meanwhile, FD transmission mode can be exploited in various scenarios to support a set of safety applications in V2V systems because FD devices can transmit signal and sense the environment simultaneously; thus, reducing the end-to-end delay of the systems [6]. Consequently, the combination of EH and FD in a V2V system can achieve many advantages such as solving the battery and spectrum efficiency issues. The main contributions of the paper is shortened as:

- We investigate an FD-EH-V2V relay system where the source is located at a fixed location while relay and destination move on the road. Besides, relay harvests energy from the source while moving and exchanging signals. Furthermore, we consider both AF and DF protocols at the relay.
- We mathematically derive the exact closed-form expressions of the ECs of the considered FD-EH-V2V relay system for both AF and DF protocols under the influences of RSI and cascade Rayleigh fading, then validate these derived expressions by Monte-Carlo simulations. We also observe that cascade Rayleigh fading results in more difficulties deriving closed-form expression than traditional channels such as Rayleigh and Nakagami.
- We investigate the performance of the FD-EH-V2V relay system in different scenarios. Numerical results reveal that the cascade Rayleigh fading hurts the ECs of the considered system compared with the Rayleigh fading. Furthermore, the EC of the DF protocol is higher than that of AF one, and the ECs of the considered system are higher than those of the HD-EH-V2V relay system for certain RSI and SNR. On the other hand, when RSI and the average transmission power of the source are fixed, a suitable time switching ratio can be chosen to maximize the ECs of the considered system.

The rest of the paper is organized as follows. Section II describes the system model of the considered FD-EH-V2V relay system with signal processing for both AF and DF protocols. Section III mathematically derives the EC expressions of the considered system. Section IV provides numerical results and discussions. Finally, Section V draws some conclusions.

II. System Model

The considered LPWA system is illustrated in Fig. 1. The system consists of a power beacon (B), a sensor (S), K gateways ($\mathrm{G}_1, \mathrm{G}_2$,..., G_K), and a server center (C). Specifically, S has only one antenna while B and G_k ($k = 1, 2, ..., K$), respectively, have M and N antennas. In addition, S is located in a restricted area, it is difficult to supply power to it. Therefore, S has to harvest the energy from B via radio frequency (RF) signals for data transmission.

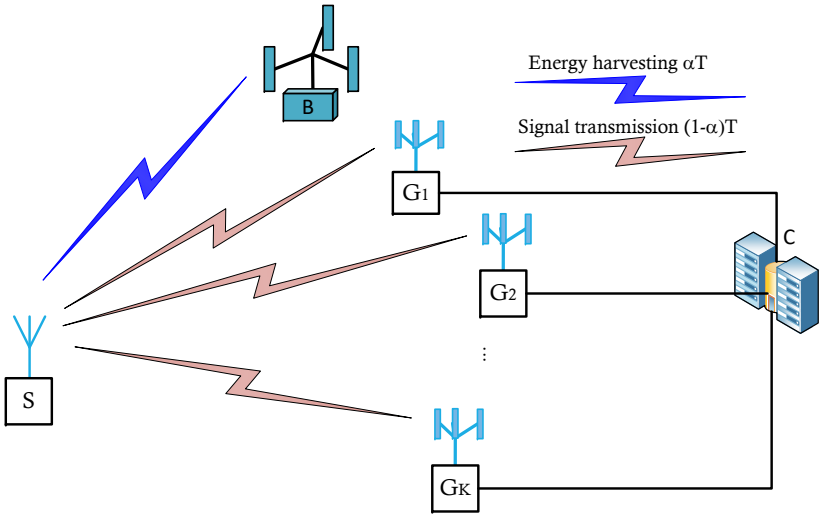

Fig. 1: Illustration of the considered LPWA system.

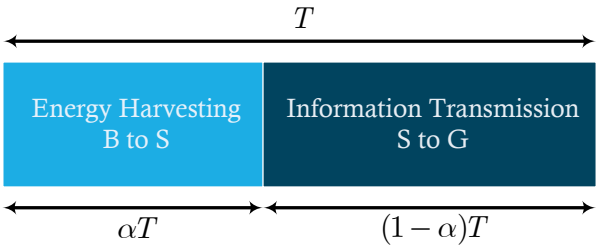

Fig. 2: TS protocol for the considered LPWA system.

There are two stages for the system operation, as shown from Fig. 2. First, S harvests energy from B using the interval αT, where α is the time switching ratio satisfying $0 \leq \alpha \leq 1$ and T is the transmission block. Second, S transmits signals to all gateways using the remain interval $(1-\alpha)T$.

In the interval of EH, the harvested energy at S with (denoted by E_S) is given as

$$E_S = \frac{\eta \alpha T P_{\rm B} d_{\rm BS}^{-\beta} \|\mathbf{h}_{\rm BS}\|^2}{M}, \tag{1}$$

where η is the energy conversion efficiency ($0 \leq \eta \leq 1$); $P_{\rm B}$ is the total transmission power of B; $d_{\rm BS}$ is the distance between B and S; $2 \leq \beta \leq 4$ is the path-loss exponent; $\mathbf{h}_{\rm BS}$ is the channel vector from M transmit antennas of B to one receive antenna of S. Then, all the harvested energy at S is transformed to the power for signal transmission. The transmit power of S is thus given as

$$P_{\rm S} = \frac{\eta \alpha T P_{\rm B} d_{\rm BS}^{-\beta} \|\mathbf{h}_{\rm BS}\|^2}{M(1-\alpha)T} = \frac{\eta \alpha P_{\rm B} \|\mathbf{h}_{\rm BS}\|^2}{M(1-\alpha) d_{\rm BS}^{\beta}}. \tag{2}$$

The received signals at G_k in the interval $(1-\alpha)T$ is computed as

$$y_{\mathrm{G}_k} = \mathbf{h}_{\mathrm{SG}_k} \sqrt{P_{\rm S} d_{\mathrm{SG}_k}^{-\beta}} x_{\rm S} + z_{\mathrm{G}_k}, \tag{3}$$

where $\mathbf{h}_{\mathrm{SG}_k}$ is the channel vector from one transmit antenna of S to N receive antennas of the kth gateway; x_{S} is the transmitted signal at S; d_{SG_k} is the distance from S to the kth gateway; z_{G_k} is the Gaussian noise at the kth gateway with zero mean and variance of σ^2, i.e., $z_{\mathrm{G}_k} \sim C\mathcal{N}(0, \sigma^2)$.

At the each gateway, maximum ratio combining (MRC) is applied to maximize the received signal power. Consequently, the signal-to-noise (SNR) ratio at the kth gateway is calculated as

$$\gamma_{\mathrm{G}_k} = \frac{\|\mathbf{h}_{\mathrm{SG}_k}\|^2 P_{\mathrm{S}} d_{\mathrm{SG}_k}^{-\beta}}{\sigma^2}. \tag{4}$$

In the case of cooperative communication, all the distances from S to all gateways are normalized for combining the signal at the server center [...]. Thus, the received signal at C is now expressed as

$$y_{\mathrm{C}} = \sqrt{P_{\mathrm{S}} \sum_{k=1}^{K} \|\mathbf{h}_{\mathrm{SG}_k}\|^2 d_0^{-\beta}} x_{\mathrm{S}} + z_{\mathrm{C}}, \tag{5}$$

where $d_0 = \min(d_{\mathrm{SG}_1}, d_{\mathrm{SG}_2}, ..., d_{\mathrm{SG}_K})$; z_{C} is the Gaussian noise term.

From (5), the SNR at C is computed as

$$\gamma_{\mathrm{C}} = \frac{P_{\mathrm{S}} \sum\limits_{k=1}^{K} \|\mathbf{h}_{\mathrm{SG}_k}\|^2 d_0^{-\beta}}{\sigma^2}. \tag{6}$$

Replacing P_{S} from (2) into (4) and (6), the SNR at the kth gateway and C are, respectively, expressed as

$$\gamma_{\mathrm{G}_k} = \frac{\eta\alpha P_{\mathrm{B}} \|\mathbf{h}_{\mathrm{BS}}\|^2 \|\mathbf{h}_{\mathrm{SG}_k}\|^2}{M\sigma^2(1-\alpha) d_{\mathrm{BS}}^{\beta} d_{\mathrm{SG}_k}^{\beta}}, \tag{7}$$

$$\gamma_{\mathrm{C}} = \frac{\eta\alpha P_{\mathrm{B}} \|\mathbf{h}_{\mathrm{BS}}\|^2 \sum\limits_{k=1}^{K} \|\mathbf{h}_{\mathrm{SG}_k}\|^2}{M\sigma^2(1-\alpha) d_{\mathrm{BS}}^{\beta} d_0^{\beta}}. \tag{8}$$

III. Performance Analysis

A. Outage Probability

The OP of the considered LPWA system is defined as the probability when the instantaneous data transmission rate is lower than the pre-defined data transmission rate. Mathematically, the OPs in the cases of without and with cooperative communication are, respectively, computed as

$$\mathcal{P}_k = \Pr\Big\{(1-\alpha)\log_2(1+\gamma_{\mathrm{G}_k}) < \mathcal{R}\Big\}, \tag{9}$$

$$\mathcal{P}_{\mathrm{C}} = \Pr\Big\{(1-\alpha)\log_2(1+\gamma_{\mathrm{C}}) < \mathcal{R}\Big\}, \tag{10}$$

where γ_{G_k} and γ_{C} are, respectively, given in (7) and (8); $\mathcal{R}$ is the pre-defined data transmission rate.

Let $\gamma_{\rm th} = 2^{\frac{\mathcal{R}}{1-\alpha}} - 1$ be the outage threshold, (9) and (10) can be rewritten as

$$\mathcal{P}_k = \Pr\Big\{\gamma_{\mathrm{G}_k} < \gamma_{\rm th}\Big\}, \tag{11}$$

$$\mathcal{P}_{\rm C} = \Pr\Big\{\gamma_{\rm C} < \gamma_{\rm th}\Big\}. \tag{12}$$

From (11) and (12), the OPs of the considered system are derived as the following Theorem 1.

Theorem 1: The OPs of the considered LPWA system with energy harvesting in the cases of non-cooperative and cooperative communication over Rayleigh fading channel are given as

$$\mathcal{P}_k = 1 - \frac{2}{\Gamma(N)}\sum_{m=0}^{M-1}\frac{1}{m!}\left(\frac{M\sigma^2(1-\alpha)d_{\rm BS}^{\beta}d_{{\rm SG}_k}^{\beta}\gamma_{\rm th}}{\eta\alpha P_{\rm B}}\right)^{\frac{N+m}{2}}\mathcal{K}_{N-m}\left(2\sqrt{\frac{M\sigma^2(1-\alpha)d_{\rm BS}^{\beta}d_{{\rm SG}_k}^{\beta}\gamma_{\rm th}}{\eta\alpha P_{\rm B}}}\right), \tag{13}$$

$$\mathcal{P}_{\rm C} = 1 - \frac{2}{\Gamma(KN)}\sum_{m=0}^{M-1}\frac{1}{m!}\left(\frac{M\sigma^2(1-\alpha)d_{\rm BS}^{\beta}d_{0}^{\beta}\gamma_{\rm th}}{\eta\alpha P_{\rm B}}\right)^{\frac{KN+m}{2}}\mathcal{K}_{KN-m}\left(2\sqrt{\frac{M\sigma^2(1-\alpha)d_{\rm BS}^{\beta}d_{0}^{\beta}\gamma_{\rm th}}{\eta\alpha P_{\rm B}}}\right), \tag{14}$$

where $\Gamma(.)$ is the gamma function; $\mathcal{K}_{N-m}(.)$ and $\mathcal{K}_{KN-m}(.)$ are, respectively, the $N-m$ and $KN-m$ order modified Bessel functions of the second kind [24].

Proof: Replacing γ_{G_k} and $\gamma_{\rm C}$ in (7) and (8) into (11) and (12), respectively, the OPs are now expressed as

$$\begin{aligned}\mathcal{P}_k &= \Pr\left\{\frac{\eta\alpha P_{\rm B}\|\mathbf{h}_{\rm BS}\|^2\|\mathbf{h}_{{\rm SG}_k}\|^2}{M\sigma^2(1-\alpha)d_{\rm BS}^{\beta}d_{{\rm SG}_k}^{\beta}} < \gamma_{\rm th}\right\}\\ &= \Pr\left\{\|\mathbf{h}_{\rm BS}\|^2\|\mathbf{h}_{{\rm SG}_k}\|^2 < \frac{M\sigma^2(1-\alpha)d_{\rm BS}^{\beta}d_{{\rm SG}_k}^{\beta}\gamma_{\rm th}}{\eta\alpha P_{\rm B}}\right\}\\ &= 1 - \int_0^{\infty}\left[1 - F_{\|\mathbf{h}_{\rm BS}\|^2}\left(\frac{M\sigma^2(1-\alpha)d_{\rm BS}^{\beta}d_{{\rm SG}_k}^{\beta}\gamma_{\rm th}}{\eta\alpha P_{\rm B}y}\right)\right]f_{\|\mathbf{h}_{{\rm SG}_k}\|^2}(y)dy,\end{aligned} \tag{15}$$

$$\begin{aligned}\mathcal{P}_{\rm C} &= \Pr\left\{\frac{\eta\alpha P_{\rm B}\|\mathbf{h}_{\rm BS}\|^2\sum\limits_{k=1}^{K}\|\mathbf{h}_{{\rm SG}_k}\|^2}{M\sigma^2(1-\alpha)d_{\rm BS}^{\beta}d_{0}^{\beta}} < \gamma_{\rm th}\right\}\\ &= \Pr\left\{\|\mathbf{h}_{\rm BS}\|^2\sum_{k=1}^{K}\|\mathbf{h}_{{\rm SG}_k}\|^2 < \frac{M\sigma^2(1-\alpha)d_{\rm BS}^{\beta}d_{0}^{\beta}\gamma_{\rm th}}{\eta\alpha P_{\rm B}}\right\}\\ &= 1 - \int_0^{\infty}\left[1 - F_{\|\mathbf{h}_{\rm BS}\|^2}\left(\frac{M\sigma^2(1-\alpha)d_{\rm BS}^{\beta}d_{0}^{\beta}\gamma_{\rm th}}{\eta\alpha P_{\rm B}z}\right)\right]f_{\sum\limits_{k=1}^{K}\|\mathbf{h}_{{\rm SG}_k}\|^2}(z)dz,\end{aligned} \tag{16}$$

where $F(.)$ and $f(.)$ are respectively the cumulative distribution function (CDF) and the probability density function (PDF) of the instantaneous channel gain amplitude.

To derive the exact closed-form expressions from (15) and (16), we firstly obtain the CDF and PDF of the instantaneous channel gain following Rayleigh distribution. For only one channel gain, i.e., $|h|^2$, the CDF and PDF are, respectively, given as

$$F_{|h|^2}(x) = 1 - \exp(-x),\ x \geq 0, \tag{17}$$

$$f_{|h|^2}(x) = \exp(-x),\ x \geq 0. \tag{18}$$

When MRT/MRC techniques are applied at the transmitter/receiver, such as MRT at power beacon and MRC at kth gateway or server center, the CDF and PDF of channel gains, i.e, $\|\mathbf{h}_{\mathrm{BS}}\|^2$ is expressed as [25]:

$$F_{\|\mathbf{h}_{\mathrm{BS}}\|^2}(x) = 1 - \exp(-x)\sum_{m=0}^{M-1}\frac{x^m}{m!}, \quad x \geq 0, \tag{19}$$

$$f_{\|\mathbf{h}_{\mathrm{BS}}\|^2}(x) = \frac{x^{M-1}\exp(-x)}{\Gamma(M)}, \quad x \geq 0. \tag{20}$$

Now, applying (19) and (20), the probabilities in (15) and (16) are solved as

$$\begin{aligned}\mathcal{P}_k &= 1 - \int_0^\infty \exp\left(-\frac{M\sigma^2(1-\alpha)d_{\mathrm{BS}}^\beta d_{\mathrm{SG}_k}^\beta \gamma_{\mathrm{th}}}{\eta\alpha P_{\mathrm{B}} y}\right)\sum_{m=0}^{M-1}\frac{1}{m!}\left(\frac{M\sigma^2(1-\alpha)d_{\mathrm{BS}}^\beta d_{\mathrm{SG}_k}^\beta \gamma_{\mathrm{th}}}{\eta\alpha P_{\mathrm{B}} y}\right)^m \frac{y^{N-1}\exp(-y)}{\Gamma(N)}dy \\ &= 1 - \frac{1}{\Gamma(N)}\sum_{m=0}^{M-1}\frac{1}{m!}\left(\frac{M\sigma^2(1-\alpha)d_{\mathrm{BS}}^\beta d_{\mathrm{SG}_k}^\beta \gamma_{\mathrm{th}}}{\eta\alpha P_{\mathrm{B}}}\right)^m \int_0^\infty \exp\left(-\frac{M\sigma^2(1-\alpha)d_{\mathrm{BS}}^\beta d_{\mathrm{SG}_k}^\beta \gamma_{\mathrm{th}}}{\eta\alpha P_{\mathrm{B}} y} - y\right)y^{N-m-1}dy, \end{aligned} \tag{21}$$

$$\begin{aligned}\mathcal{P}_{\mathrm{C}} &= 1 - \int_0^\infty \exp\left(-\frac{M\sigma^2(1-\alpha)d_{\mathrm{BS}}^\beta d_0^\beta \gamma_{\mathrm{th}}}{\eta\alpha P_{\mathrm{B}} z}\right)\sum_{m=0}^{M-1}\frac{1}{m!}\left(\frac{M\sigma^2(1-\alpha)d_{\mathrm{BS}}^\beta d_0^\beta \gamma_{\mathrm{th}}}{\eta\alpha P_{\mathrm{B}} z}\right)^m \frac{z^{KN-1}\exp(-z)}{\Gamma(KN)}dz \\ &= 1 - \frac{1}{\Gamma(KN)}\sum_{m=0}^{M-1}\frac{1}{m!}\left(\frac{M\sigma^2(1-\alpha)d_{\mathrm{BS}}^\beta d_0^\beta \gamma_{\mathrm{th}}}{\eta\alpha P_{\mathrm{B}}}\right)^m \int_0^\infty \exp\left(-\frac{M\sigma^2(1-\alpha)d_{\mathrm{BS}}^\beta d_0^\beta \gamma_{\mathrm{th}}}{\eta\alpha P_{\mathrm{B}} z} - z\right)z^{KN-m-1}dz. \end{aligned} \tag{22}$$

Applying [24, Eq. (3.471.9)], two above integrals are computed as

$$\begin{aligned}&\int_0^\infty \exp\left(-\frac{M\sigma^2(1-\alpha)d_{\mathrm{BS}}^\beta d_{\mathrm{SG}_k}^\beta \gamma_{\mathrm{th}}}{\eta\alpha P_{\mathrm{B}} y} - y\right)y^{N-m-1}dy \\ &= 2\left(\frac{M\sigma^2(1-\alpha)d_{\mathrm{BS}}^\beta d_{\mathrm{SG}_k}^\beta \gamma_{\mathrm{th}}}{\eta\alpha P_{\mathrm{B}}}\right)^{\frac{N-m}{2}}\mathcal{K}_{N-m}\left(2\sqrt{\frac{M\sigma^2(1-\alpha)d_{\mathrm{BS}}^\beta d_{\mathrm{SG}_k}^\beta \gamma_{\mathrm{th}}}{\eta\alpha P_{\mathrm{B}}}}\right), \end{aligned} \tag{23}$$

$$\begin{aligned}&\int_0^\infty \exp\left(-\frac{M\sigma^2(1-\alpha)d_{\mathrm{BS}}^\beta d_0^\beta \gamma_{\mathrm{th}}}{\eta\alpha P_{\mathrm{B}} z} - z\right)z^{KN-m-1}dz \\ &= 2\left(\frac{M\sigma^2(1-\alpha)d_{\mathrm{BS}}^\beta d_0^\beta \gamma_{\mathrm{th}}}{\eta\alpha P_{\mathrm{B}}}\right)^{\frac{KN-m}{2}}\mathcal{K}_{KN-m}\left(2\sqrt{\frac{M\sigma^2(1-\alpha)d_{\mathrm{BS}}^\beta d_0^\beta \gamma_{\mathrm{th}}}{\eta\alpha P_{\mathrm{B}}}}\right). \end{aligned} \tag{24}$$

Replacing (23) and (24) into (21) and (22), respectively, we obtain the exact closed-form expressions of OPs of the considered LPWA system as in Theorem 1. The proof is now complete.

B. Symbol Error Probability

The SEP of the considered LPWA system is expressed as

$$\mathrm{SEP} = a\mathbb{E}\{Q(\sqrt{b\gamma})\} = \frac{a}{\sqrt{2\pi}}\int_0^\infty F\left(\frac{t^2}{b}\right)e^{-\frac{t^2}{2}}dt, \tag{25}$$

where (a, b) is a couple of the modulation types, i.e., $(a, b) = (1, 2)$ and $(a, b) = (2, 1)$ for the binary phase-shift keying (BPSK) and 4-quadrature amplitude modulation (4-QAM), respectively [26]; $Q(x)$ denotes the Gaussian function; γ is SNR of

the considered system, which is given as (7) and (8) for the cases without and with cooperative communication, respectively. By changing variable, i.e., $x = \frac{t^2}{b}$, (25) can be rewritten as

$$\mathrm{SEP} = \frac{a\sqrt{b}}{2\sqrt{2\pi}} \int_0^\infty \frac{F(x)}{\sqrt{x}} \exp\Big(-\frac{bx}{2}\Big) dx. \tag{26}$$

Based on (26), the SEPs of the considered LPWA system are derived in the following Theorem 2.

Theorem 2: The SEPs of the considered LPWA system with energy harvesting in the cases of non-cooperative and cooperative communication over Rayleigh fading channel are, respectively, given as

$$\begin{aligned}\mathrm{SEP}_k =& \frac{a\sqrt{b}}{2\sqrt{2\pi}} \Bigg[\sqrt{\frac{2\pi}{b}} - \frac{1}{\Gamma(N)} \Gamma\Big(N+\frac{1}{2}\Big) \exp\left(\frac{M\sigma^2(1-\alpha) d_{\mathrm{BS}}^\beta d_{\mathrm{SG}_k}^\beta}{b\eta\alpha P_{\mathrm{B}}}\right) \\ & \times \sum_{m=0}^{M-1} \frac{\Gamma\Big(m+\frac{1}{2}\Big)}{m!} \Big(\frac{b}{2}\Big)^{\frac{N+m}{2}} \left(\frac{M\sigma^2(1-\alpha) d_{\mathrm{BS}}^\beta d_{\mathrm{SG}_k}^\beta}{\eta\alpha P_{\mathrm{B}}}\right)^{\frac{N+m-1}{2}} \mathcal{W}_{-\frac{N+m}{2}, \frac{N-m}{2}} \left(\frac{2M\sigma^2(1-\alpha) d_{\mathrm{BS}}^\beta d_{\mathrm{SG}_k}^\beta}{b\eta\alpha P_{\mathrm{B}}}\right) \Bigg], \end{aligned} \tag{27}$$

$$\begin{aligned}\mathrm{SEP}_{\mathrm{C}} =& \frac{a\sqrt{b}}{2\sqrt{2\pi}} \Bigg[\sqrt{\frac{2\pi}{b}} - \frac{1}{\Gamma(KN)} \Gamma\Big(KN+\frac{1}{2}\Big) \exp\left(\frac{M\sigma^2(1-\alpha) d_{\mathrm{BS}}^\beta d_0^\beta}{b\eta\alpha P_{\mathrm{B}}}\right) \\ & \times \sum_{m=0}^{M-1} \frac{\Gamma\Big(m+\frac{1}{2}\Big)}{m!} \Big(\frac{b}{2}\Big)^{\frac{KN+m}{2}} \left(\frac{M\sigma^2(1-\alpha) d_{\mathrm{BS}}^\beta d_0^\beta}{\eta\alpha P_{\mathrm{B}}}\right)^{\frac{KN+m-1}{2}} \mathcal{W}_{-\frac{KN+m}{2}, \frac{KN-m}{2}} \left(\frac{2M\sigma^2(1-\alpha) d_{\mathrm{BS}}^\beta d_0^\beta}{b\eta\alpha P_{\mathrm{B}}}\right) \Bigg], \end{aligned} \tag{28}$$

where $\mathcal{W}_{.,.}(.)$ is the Whittaker functions [24].

Proof: To obtain the SEPs of the considered LPWA system, we firstly derive the CDF, $F(x)$ in the cases of non-cooperative and cooperative communications. Based on the definition of $F(x)$, i.e.,

$$F(x) = \Pr\{\gamma < x\}, \tag{29}$$

we can easily obtain the CDFs of the considered LPWA system in the cases of non-cooperative and cooperative communications by replacing γ_{th} by x in the OP expressions. Therefore, the CDFs in the cases of non-cooperative ($F_k(x)$) and cooperative ($F_{\mathrm{C}}(x)$) communications are, respectively, derived as

$$F_k(x) = 1 - \frac{2}{\Gamma(N)} \sum_{m=0}^{M-1} \frac{1}{m!} \left(\frac{M\sigma^2(1-\alpha) d_{\mathrm{BS}}^\beta d_{\mathrm{SG}_k}^\beta x}{\eta\alpha P_{\mathrm{B}}}\right)^{\frac{N+m}{2}} \mathcal{K}_{N-m}\left(2\sqrt{\frac{M\sigma^2(1-\alpha) d_{\mathrm{BS}}^\beta d_{\mathrm{SG}_k}^\beta x}{\eta\alpha P_{\mathrm{B}}}}\right), \tag{30}$$

$$F_{\mathrm{C}}(x) = 1 - \frac{2}{\Gamma(KN)} \sum_{m=0}^{M-1} \frac{1}{m!} \left(\frac{M\sigma^2(1-\alpha) d_{\mathrm{BS}}^\beta d_0^\beta x}{\eta\alpha P_{\mathrm{B}}}\right)^{\frac{KN+m}{2}} \mathcal{K}_{KN-m}\left(2\sqrt{\frac{M\sigma^2(1-\alpha) d_{\mathrm{BS}}^\beta d_0^\beta x}{\eta\alpha P_{\mathrm{B}}}}\right). \tag{31}$$

Replacing (30) and (31), the SEPs are now expressed as

$$\begin{aligned}\mathrm{SEP}_k =& \frac{a\sqrt{b}}{2\sqrt{2\pi}} \int_0^\infty \frac{\exp\Big(-\frac{bx}{2}\Big)}{\sqrt{x}} \left[1 - \frac{2}{\Gamma(N)} \sum_{m=0}^{M-1} \frac{1}{m!} \left(\frac{M\sigma^2(1-\alpha) d_{\mathrm{BS}}^\beta d_{\mathrm{SG}_k}^\beta x}{\eta\alpha P_{\mathrm{B}}}\right)^{\frac{N+m}{2}} \mathcal{K}_{N-m}\left(2\sqrt{\frac{M\sigma^2(1-\alpha) d_{\mathrm{BS}}^\beta d_{\mathrm{SG}_k}^\beta x}{\eta\alpha P_{\mathrm{B}}}}\right)\right] dx \\ =& \frac{a\sqrt{b}}{2\sqrt{2\pi}} \Bigg[\int_0^\infty \frac{\exp\Big(-\frac{bx}{2}\Big)}{\sqrt{x}} dx - \frac{2}{\Gamma(N)} \sum_{m=0}^{M-1} \frac{1}{m!} \left(\frac{M\sigma^2(1-\alpha) d_{\mathrm{BS}}^\beta d_{\mathrm{SG}_k}^\beta}{\eta\alpha P_{\mathrm{B}}}\right)^{\frac{N+m}{2}} \\ & \times \int_0^\infty x^{\frac{N+m-1}{2}} \exp\Big(-\frac{bx}{2}\Big) \mathcal{K}_{N-m}\left(2\sqrt{\frac{M\sigma^2(1-\alpha) d_{\mathrm{BS}}^\beta d_{\mathrm{SG}_k}^\beta x}{\eta\alpha P_{\mathrm{B}}}}\right) dx \Bigg]. \end{aligned} \tag{32}$$

$$\begin{aligned}\mathrm{SEP_C} =&\frac{a\sqrt{b}}{2\sqrt{2\pi}}\int_0^\infty \frac{\exp\Big(-\frac{bx}{2}\Big)}{\sqrt{x}}\left[1-\frac{2}{\Gamma(KN)}\sum_{m=0}^{M-1}\frac{1}{m!}\left(\frac{M\sigma^2(1-\alpha)d_{\mathrm{BS}}^{\beta}d_0^{\beta}x}{\eta\alpha P_{\mathrm{B}}}\right)^{\frac{KN+m}{2}}\mathcal{K}_{KN-m}\left(2\sqrt{\frac{M\sigma^2(1-\alpha)d_{\mathrm{BS}}^{\beta}d_0^{\beta}x}{\eta\alpha P_{\mathrm{B}}}}\right)\right]dx\\ =&\frac{a\sqrt{b}}{2\sqrt{2\pi}}\left[\int_0^\infty \frac{\exp\Big(-\frac{bx}{2}\Big)}{\sqrt{x}}dx-\frac{2}{\Gamma(KN)}\sum_{m=0}^{M-1}\frac{1}{m!}\left(\frac{M\sigma^2(1-\alpha)d_{\mathrm{BS}}^{\beta}d_0^{\beta}}{\eta\alpha P_{\mathrm{B}}}\right)^{\frac{KN+m}{2}}\right.\\ &\left.\times\int_0^\infty x^{\frac{KN+m-1}{2}}\exp\Big(-\frac{bx}{2}\Big)\mathcal{K}_{KN-m}\left(2\sqrt{\frac{M\sigma^2(1-\alpha)d_{\mathrm{BS}}^{\beta}d_0^{\beta}x}{\eta\alpha P_{\mathrm{B}}}}\right)dx\right].\end{aligned}\tag{33}$$

Applying [24, Eq. (6.643.3)], two integrals in (32) and (33) are now calculated as

Replacing (**??**) into (**??**), we obtain the EC of the considered system with AF protocol as (**??**).

For DF protocol, the CDF of γ_{DF} (denoted by $F_{\mathrm{DF}}(x)$) is computed as

$$F_{\mathrm{DF}}(x)=\Pr\left\{\gamma_{\mathrm{DF}}<x\right\}=\Pr\left\{\min(\gamma_{\mathrm{R}},\gamma_{\mathrm{D}})<x\right\}=1-\Pr\left\{\gamma_{\mathrm{R}}>x,\gamma_{\mathrm{D}}>x\right\}.\tag{34}$$

Substituting γ_{R} and γ_{D} in (**??**) and (**??**) into (34), we have

$$\begin{aligned}F_{\mathrm{DF}}(x)&=1-\Pr\left\{\frac{|h_{\mathrm{SR}}|^2P_{\mathrm{S}}}{\sigma_{\mathrm{RSI}}^2+\sigma_{\mathrm{R}}^2}>x,\frac{|h_{\mathrm{SR}}|^2|h_{\mathrm{RD}}|^2\eta\alpha P_{\mathrm{S}}}{\sigma_{\mathrm{D}}^2(1-\alpha)}>x\right\}\\ &=1-\Pr\left\{|h_{\mathrm{SR}}|^2>\frac{x(\sigma_{\mathrm{RSI}}^2+\sigma_{\mathrm{R}}^2)}{P_{\mathrm{S}}},|h_{\mathrm{RD}}|^2>\frac{x\sigma_{\mathrm{D}}^2(1-\alpha)}{|h_{\mathrm{SR}}|^2\eta\alpha P_{\mathrm{S}}}\right\}\\ &=1-\left(1-\Pr\left\{|h_{\mathrm{RD}}|^2\le\frac{x\sigma_{\mathrm{D}}^2(1-\alpha)}{|h_{\mathrm{SR}}|^2\eta\alpha P_{\mathrm{S}}}\Big|_{|h_{\mathrm{SR}}|^2>\frac{x(\sigma_{\mathrm{RSI}}^2+\sigma_{\mathrm{R}}^2)}{P_{\mathrm{S}}}}\right\}\right).\end{aligned}\tag{35}$$

Using the conditional probability [27], (35) can be expressed as

$$F_{\mathrm{DF}}(x)=1-\int_0^\infty\left(1-F_{|h_{\mathrm{RD}}|^2}\Big(\frac{x\sigma_{\mathrm{D}}^2(1-\alpha)}{|h_{\mathrm{SR}}|^2\eta\alpha P_{\mathrm{S}}}\Big)\right)f_{|h_{\mathrm{SR}}|^2}\Big(y+\frac{x(\sigma_{\mathrm{RSI}}^2+\sigma_{\mathrm{R}}^2)}{P_{\mathrm{S}}}\Big)dy,\tag{36}$$

where $y=|h_{\mathrm{SR}}|^2-\frac{x(\sigma_{\mathrm{RSI}}^2+\sigma_{\mathrm{R}}^2)}{P_{\mathrm{S}}}$.

Applying (**??**) and (**??**), (36) becomes

$$\begin{aligned}F_{\mathrm{DF}}(x)&=1-\int_0^\infty\sqrt{\frac{4x\sigma_{\mathrm{D}}^2(1-\alpha)}{\Big(y+\frac{x(\sigma_{\mathrm{RSI}}^2+\sigma_{\mathrm{R}}^2)}{P_{\mathrm{S}}}\Big)\eta\alpha P_{\mathrm{S}}}}K_1\left(\sqrt{\frac{4x\sigma_{\mathrm{D}}^2(1-\alpha)}{\Big(y+\frac{x(\sigma_{\mathrm{RSI}}^2+\sigma_{\mathrm{R}}^2)}{P_{\mathrm{S}}}\Big)\eta\alpha P_{\mathrm{S}}}}\right)\exp\Big(-y-\frac{x(\sigma_{\mathrm{RSI}}^2+\sigma_{\mathrm{R}}^2)}{P_{\mathrm{S}}}\Big)dy\\ &=1-\int_0^\infty\sqrt{\frac{\Phi x}{y+\Psi x}}K_1\left(\sqrt{\frac{\Phi x}{y+\Psi x}}\right)\exp\Big(-y-\Psi x\Big)dy\\ &=1-\exp(-\Psi x)\int_0^\infty\sqrt{\frac{\Phi x}{y+\Psi x}}K_1\left(\sqrt{\frac{\Phi x}{y+\Psi x}}\right)\exp(-y)dy.\end{aligned}\tag{37}$$

Applying all steps used for AF protocol such as changing variable $z=\exp(-y)$ and using [28, Eq. (25.4.30)], we can obtain the CDF of the considered system with DF protocol as

$$F_{\mathrm{DF}}(x)=1-\frac{\pi}{2M}\exp(-\Psi x)\sum_{m=1}^{M}\sqrt{1-\phi_m^2}\sqrt{\frac{\Phi x}{\Psi x-\ln u}}K_1\left(\sqrt{\frac{\Phi x}{\Psi x-\ln u}}\right).\tag{38}$$

Then, substituting (38) into (**??**) and applying similar transformations used for AF protocol, we obtain the EC of the considered system with DF protocol as (**??**). The proof is complete.

IV. Numerical Results and Discussions

In this section, the mathematical expressions in the previous section are used to evaluate the ECs of the considered FD-EH-V2V relay system with AF/DF protocols. The effect of several system parameters such as RSI level, the average transmission power, time switching ratio, and the cascade Rayleigh fading are investigated to provide the system deployment guidelines in practice. All mathematical expressions are validated through Monte-Carlo simulations. In particular, we use MATLAB simulator to obtain the simulation results. To generate a cascade Rayleigh fading channel, we generate two independent Rayleigh fading channels and then multiply these two channels. To realize the ECs of the HD-EH-V2V relay systems, we set the RSI level $k = 0$ in the obtain EC expressions of the FD-EH-V2V relay systems and divide the results by two because HD-EH-V2V relay systems need two time slots to transmit signal from S to D via R. In all scenarios, we set $\sigma_{\rm R}^2 = \sigma_{\rm D}^2 = \sigma^2$, the energy harvesting efficiency $\eta = 0.85$, and the complexity-accuracy trade-off parameters $M = N = 20$. In addition, the average transmission power is calculated as SNR = $P_{\rm S}/\sigma^2$. Furthermore, ECs of the considered system are compared with those in the case of Rayleigh fading channel and HD transmission mode to demonstrate the benefits of the FD technique and the impacts of the RSI and cascade Rayleigh fading. For the sake of redoing the simulation easily by other researchers, we summarize the parameter settings for evaluating the system performance in Tab. I.

TABLE I: Parameter settings for evaluating the system performance.

Notation	**Description**	**Fixed value**	**Varying range**
SNR	Signal-to-noise ratio	40 dB	10, 20, 30, 50 dB; $0 \sim 50$ dB
σ^2	Variance of Gaussian noise	1	none
η	Energy harvesting efficiency	0.85	none
α	Time switching ratio	0.5	$0.1 \sim 0.9$
k	RSI level	-20 dB	-10, -30 dB; $0 \sim 0.2$
M, N	Trade-off parameters	20	none

Fig. 3 illustrates the ECs of the considered FD-EH-V2V relay system versus the average SNR for different values of RSI level, i.e., $k = -30, -20, -10$ dB. The time switching ratio is $\alpha = 0.5$. We use (**??**) and (**??**) in the Theorem to plot the ECs of the considered FD-EH-V2V relay system with AF and DF protocols. In Fig. 3, the ECs of the FD-EH system over Rayleigh fading channels are denoted by "Sim-R". As shown in Fig. 3, the cascade Rayleigh fading reduces the ECs compared with the Rayleigh fading, especially in low SNR regime and low RSI level. Particularly, when RSI is low, i.e., $k = -30$ dB, the ECs of the considered system are 0.2 bit/s/Hz lower than those in the case Rayleigh fading for both AF and DF protocols at

SNR = 30 dB. However, all ECs approximate 9 bit/s/Hz at SNR = 50 dB. With higher RSI levels, i.e., $k = -20, -10$ dB, all ECs reach the capacity ceilings at SNR = 40 dB and 50 dB for the case $k = -10$ dB and $k = -20$ dB, respectively. In these two cases, the ECs only reach 3.1 and 6 bit/s/Hz for $k = -10$ dB and $k = -20$ dB, respectively. These features indicate a strong impact of RSI on the ECs of the considered FD-EH-V2V relay system. On the other hand, the ECs with DF protocol are always higher than those with AF protocol. This result is reasonable because AF amplifies not only noise but also the RSI.

Fig. 4 investigates the effect of the RSI on the ECs of the considered FD-EH-V2V relay system for different average transmission power, i.e., SNR = 10, 20, 30, 40 dB. We also provide the ECs of the considered system with HD transmission mode to clearly show the impact of RSI and the benefit of FD transmission mode. It is evident from Fig. 4 that the effect of RSI is significantly for high SNRs. Specifically, when self-interference is obliterated ($k = 0$), the ECs of the FD-EH-V2V relay system are two times higher than the ECs of HD-EH-V2V relay system. When k increases, the ECs of the considered FD-EH-V2V relay system decrease. In particular, the ECs of the FD-EH-V2V relay system is always higher than ECs of the HD-EH-V2V relay system for low SNRs, i.e., SNR = 10, 20 dB. However, for higher SNRs, i.e., SNR = 30, 40 dB, the ECs of the FD-EH-V2V relay system are higher or lower than the ECs of HD-EH-V2V relay system. For example, the ECs of the FD-EH-V2V relay system are higher than the ECs of the HD-EH-V2V relay system when k ranges from 0 to 0.07 and SNR = 30 dB. When $k > 0.07$, the ECs of the FD-EH-V2V relay system are lower than the ECs of the HD-EH-V2V relay system. With higher SNR, i.e., SNR = 40 dB, the ECs of the FD-EH-V2V relay system are only higher than those of the HD-EH-V2V relay system when $k < 0.03$. Therefore, depending on the measured and experimented RSI levels in practice, we can select FD or HD transmission mode to obtain high system capacity.

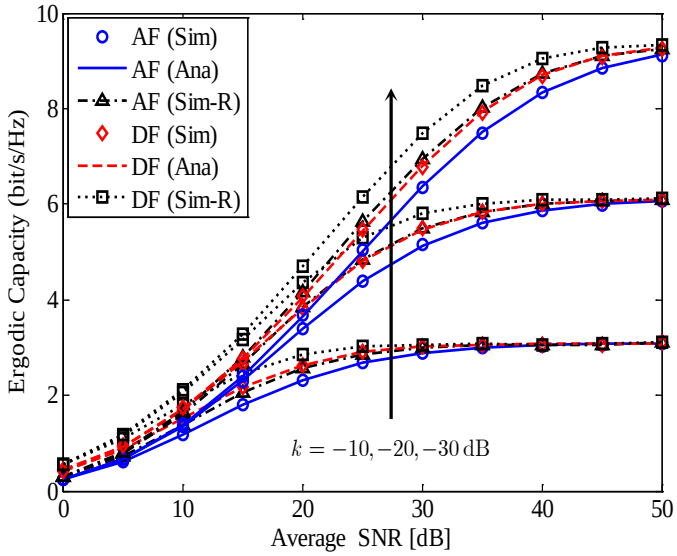

Fig. 3: The ECs of the considered FD-EH-V2V relay system for different values of RSI level, $k = -30, -20, -10$ dB; $\alpha = 0.5$.

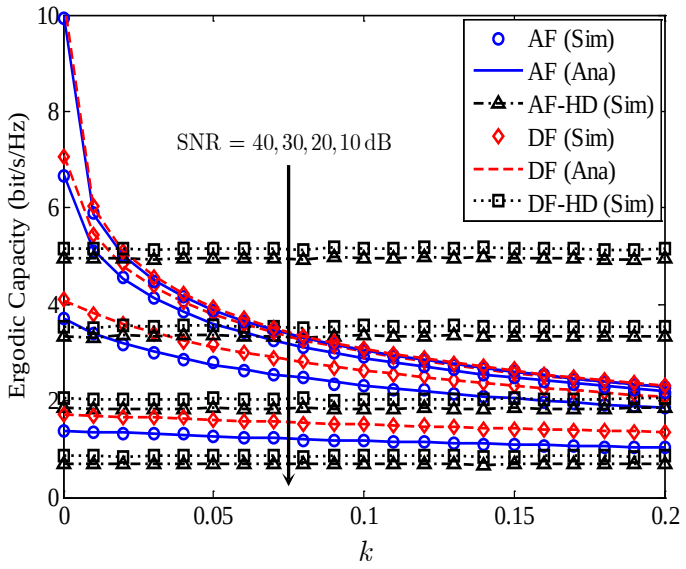

Fig. 4: The impact of RSI on the ECs of the considered FD-EH-V2V relay system for different average transmission power, SNR = 10, 20, 30, 40 dB; $\alpha = 0.5$.

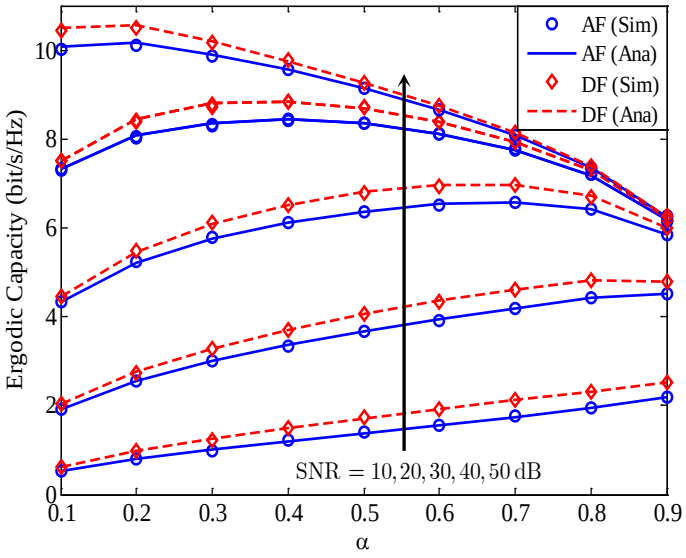

Fig. 5: The ECs of the considered FD-EH-V2V relay system versus the time switching ratio α for different SNRs, $k = -30$ dB.

Fig. 5 shows the ECs of the considered FD-EH-V2V relay system versus the time switching ratio α for different SNRs, e.g., SNR = 10, 20, 30, 40, 50 dB. The RSI level is $k = -30$ dB. As observed in Fig. 5, it is obvious that the ECs of the considered FD-EH-V2V relay system closely depend on α. When SNR is small, i.e., SNR = 10, 20 dB, the ECs increase with α. It is because small SNR means low transmission power of S; thus, R needs more time for EH to have enough signal transmission power. However, when SNR is higher, i.e., SNR = 30, 40, 50 dB, the ECs firstly increase and then decrease when

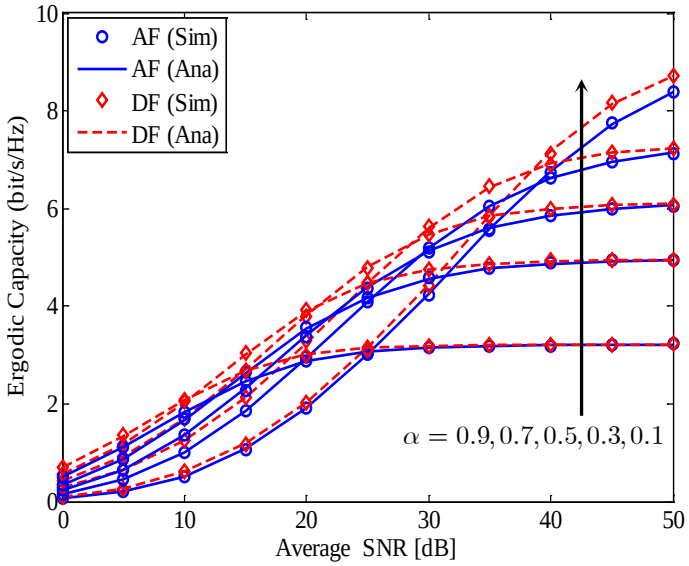

Fig. 6: The ECs of the considered FD-EH-V2V relay system versus the average SNR for different values of time switching ratio, $k = -20$ dB.

α gets higher. Specifically, for SNR = 30 dB and SNR = 40 dB, ECs are maximal when $\alpha = 0.7$ and $\alpha = 0.4$, respectively, for both AF and DF protocols. If the transmission power of S continues to increase, i.e., SNR = 50 dB, ECs are maximal when $\alpha = 0.2$. Therefore, based on the transmission power of S, the optimal α can be used to obtain the peak ECs of the considered FD-EH-V2V relay system.

To understand the relationship between the average transmission power of source and the time switching ratio α, we plot the ECs of the considered FD-EH-V2V relay system versus the average SNR for various time switching ratio, $\alpha = 0.1, 0.3, 0.5, 0.7, 0.9$, as shown in Fig. 6. We can see that, in low SNR regime, i.e., SNR $<$ 20 dB, the EC of the case $\alpha = 0.7$ is the best while the EC of the case $\alpha = 0.1$ is the worst. However, for higher SNR range, 20 $<$ SNR $<$ 40 dB, the EC of the case $\alpha = 0.3$ is the best while the EC of the case $\alpha = 0.9$ is the worst. If the average SNR still increases, i.e., SNR $>$ 40 dB, the EC of the case $\alpha = 0.1$ is the best while the EC of the case $\alpha = 0.9$ is still the worst. To sum up, low SNR leads to a high α and vice versa.

The joint and cross impacts of the RSI level k and the time switching ratio α on the ECs of the considered FD-EH-V2V relay system are illustrated in Fig. 7, where the average SNR is set as SNR = 40 dB. Similar to the ECs in Fig. 5, with a certain value of k, there is an optimal α that maximizes ECs of AF/DF protocols. In particular, when $k = 0.01$, the ECs reach the maximum of 6.9 and 7.3 bit/s/Hz for AF and DF protocols, respectively, at $\alpha = 0.15$. However, with higher value of k, the ECs are highest when $\alpha = 0.1$. In other words, for k ranges from 0.02 to 0.2, ECs of AF/DF protocols decrease when α increases. Surprisingly, in the case of perfect SIC ($k = 0$), the ECs increase when α increases. As a result, besides reducing the

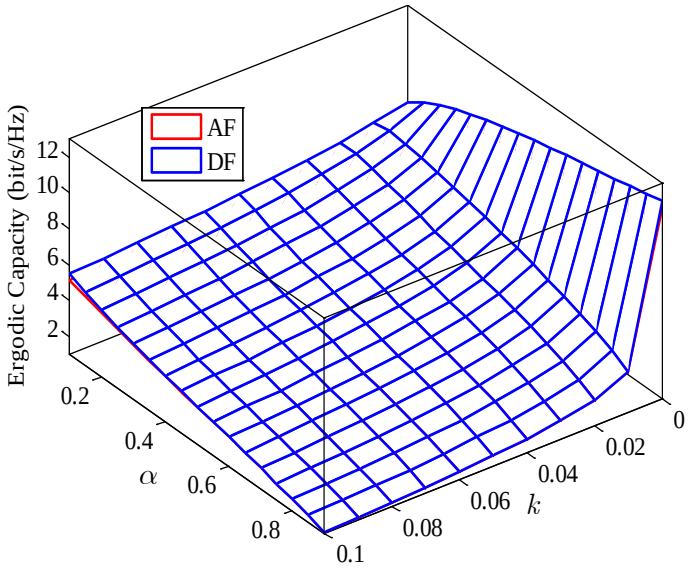

Fig. 7: The joint impacts of RSI level k and the time switching ratio α on the ECs of the considered FD-EH-V2V relay system.

ECs of the considered FD-EH-V2V relay system, the RSI also influences the optimal ECs. Therefore, for choosing an optimal α that maximizes the ECs of the considered system, it is necessary to know the RSI level and the average transmission power of the source before deploying this system in practice.

V. Conclusion

Applying FD and EH techniques are inevitable for future wireless networks, especially for V2V communication systems, because of the big advantages of these techniques. Therefore, in this paper, we evaluate the ergodic capacities of an FD-EH-V2V relay system with both AF and DF protocols under the impact of RSI and cascade Rayleigh fading channel. We mathematically derive the exact closed-form expressions of the EC of both AF and DF protocols. Numerical results reveal that the EC of DF protocol is slightly higher than that of AF one. Also, the cascade Rayleigh fading reduces the ECs of the considered system compared with the traditional Rayleigh fading. Furthermore, the ECs of the considered system are compared with those in the case of HD transmission mode to demonstrate the benefit of the FD technique. We also observe that, based on the RSI level and the source's average transmission power, we can choose an optimal time switching ratio to maximize the ECs of the considered FD-EH-V2V relay system.

Data Availability

The data used to support the findings of this study are available from the corresponding author upon request.

Conflicts of Interest

The authors declare that they have no conflicts of interest.

REFERENCES

[1] Y. Zhao, "A survey of 6G wireless communications: Emerging technologies," *arXiv preprint arXiv:2004.08549*, 2020.

[2] M. Babaei, Ü. Aygölü, M. Başaran, and L. Durak-Ata, "BER performance of full-duplex cognitive radio network with nonlinear energy harvesting," *IEEE Transactions on Green Communications and Networking*, vol. 4, no. 2, pp. 448–460, 2020.

[3] Q.-V. Pham, F. Fang, V. N. Ha, M. J. Piran, M. Le, L. B. Le, W.-J. Hwang, and Z. Ding, "A survey of multi-access edge computing in 5G and beyond: Fundamentals, technology integration, and state-of-the-art," *IEEE Access*, vol. 8, pp. 116 974–117 017, 2020.

[4] B. Clerckx, R. Zhang, R. Schober, D. W. K. Ng, D. I. Kim, and H. V. Poor, "Fundamentals of wireless information and power transfer: From RF energy harvester models to signal and system designs," *IEEE Journal on Selected Areas in Communications*, vol. 37, no. 1, pp. 4–33, 2018.

[5] H. H. M. Tam, H. D. Tuan, A. A. Nasir, T. Q. Duong, and H. V. Poor, "MIMO energy harvesting in full-duplex multi-user networks," *IEEE Transactions on Wireless Communications*, vol. 16, no. 5, pp. 3282–3297, 2017.

[6] A. H. Gazestani, S. A. Ghorashi, B. Mousavinasab, and M. Shikh-Bahaei, "A survey on implementation and applications of full duplex wireless communications," *Physical Communication*, vol. 34, pp. 121–134, 2019.

[7] Y. Deng, K. J. Kim, T. Q. Duong, M. Elkashlan, G. K. Karagiannidis, and A. Nallanathan, "Full-duplex spectrum sharing in cooperative single carrier systems," *IEEE Transactions on Cognitive Communications and Networking*, vol. 2, no. 1, pp. 68–82, 2016.

[8] B. C. Nguyen, X. N. Tran *et al.*, "On the performance of roadside unit-assisted energy harvesting full-duplex amplify-and-forward vehicle-to-vehicle relay systems," *AEU-International Journal of Electronics and Communications*, p. 153289, 2020.

[9] N.-P. Nguyen, C. Kundu, H. Q. Ngo, T. Q. Duong, and B. Canberk, "Secure full-duplex small-cell networks in a spectrum sharing environment," *IEEE Access*, vol. 4, pp. 3087–3099, 2016.

[10] B. C. Nguyen, N. N. Thang, T. M. Hoang *et al.*, "Analysis of outage probability and throughput for energy harvesting full-duplex decode-and-forward vehicle-to-vehicle relay system," *Wireless Communications and Mobile Computing*, vol. 2020, 2020.

[11] Y. Alsaba, C. Y. Leow, and S. K. A. Rahim, "Full-duplex cooperative non-orthogonal multiple access with beamforming and energy harvesting," *IEEE Access*, vol. 6, pp. 19 726–19 738, 2018.

[12] A. Koc, I. Altunbas, and E. Basar, "Two-way full-duplex spatial modulation systems with wireless powered AF relaying," *IEEE Wireless Communications Letters*, vol. 7, no. 3, pp. 444–447, 2018.

[13] C. Guo, L. Zhao, C. Feng, Z. Ding, and H.-H. Chen, "Energy harvesting enabled NOMA systems with full-duplex relaying," *IEEE Transactions on Vehicular Technology*, vol. 68, no. 7, pp. 7179–7183, 2019.

[14] T. M. Hoang, V. Van Son, N. C. Dinh, and P. T. Hiep, "Optimizing duration of energy harvesting for downlink NOMA full-duplex over nakagami-m fading channel," *AEU-international Journal of Electronics and Communications*, vol. 95, pp. 199–206, 2018.

[15] C. Li, Z. Chen, Y. Wang, Y. Yao, and B. Xia, "Outage analysis of the full-duplex decode-and-forward two-way relay system," *IEEE Trans. Veh. Technol.*, vol. 66, no. 5, pp. 4073–4086, 2017.

[16] B. C. Nguyen, X. N. Tran, D. T. Tran, and L. T. Dung, "Full-duplex amplify-and-forward relay system with direct link: Performance analysis and optimization," *Physical Communication*, vol. 37, p. 100888, 2019.

[17] X.-T. Doan, N.-P. Nguyen, C. Yin, D. B. Da Costa, and T. Q. Duong, "Cognitive full-duplex relay networks under the peak interference power constraint of multiple primary users," *EURASIP Journal on Wireless Communications and Networking*, vol. 2017, no. 1, p. 8, 2017.

[18] V.-D. Nguyen, T. Q. Duong, H. D. Tuan, O.-S. Shin, and H. V. Poor, "Spectral and energy efficiencies in full-duplex wireless information and power transfer," *IEEE Transactions on Communications*, vol. 65, no. 5, pp. 2220–2233, 2017.

[19] D. H. Chen and Y. C. He, "Full-duplex secure communications in cellular networks with downlink wireless power transfer," *IEEE Transactions on Communications*, vol. 66, no. 1, pp. 265–277, 2018.

[20] C. Campolo, A. Molinaro, A. O. Berthet, and A. Vinel, "Full-duplex radios for vehicular communications," *IEEE Communications Magazine*, vol. 55, no. 6, pp. 182–189, 2017.

[21] M. Yang, S.-W. Jeon, and D. K. Kim, "Interference management for in-band full-duplex vehicular access networks," *IEEE Transactions on Vehicular Technology*, vol. 67, no. 2, pp. 1820–1824, 2018.

[22] Y. Ai, M. Cheffena, A. Mathur, and H. Lei, "On physical layer security of double rayleigh fading channels for vehicular communications," *IEEE Wireless Communications Letters*, vol. 7, no. 6, pp. 1038–1041, 2018.

[23] R. Atallah, M. Khabbaz, and C. Assi, "Energy harvesting in vehicular networks: A contemporary survey," *IEEE Wireless Communications*, vol. 23, no. 2, pp. 70–77, 2016.

[24] A. Jeffrey and D. Zwillinger, *Table of integrals, series, and products*. Academic Press, 2007.

[25] B. C. Nguyen, N. N. Thang, X. N. Tran *et al.*, "Impacts of imperfect channel state information, transceiver hardware, and self-interference cancellation on the performance of full-duplex MIMO relay system," *Sensors*, vol. 20, no. 6, p. 1671, 2020.

[26] A. Goldsmith, *Wireless communications*. Cambridge university press, 2005.

[27] A. Leon-Garcia and A. Leon-Garcia, *Probability, statistics, and random processes for electrical engineering*. Pearson/Prentice Hall 3rd ed. Upper Saddle River, NJ, 2008.

[28] M. Abramowitz and I. A. Stegun, *Handbook of mathematical functions with formulas, graphs, and mathematical tables*. Dover, New York, 1972, vol. 9.